XI International Conference on Computational Plasticity. Fundamentals and Applications
COMPLAS XI
E. Oñate, D.R.J. Owen, D. Peric and B. Suárez (Eds)

CRACK PROPAGATION IN SHELLS DUE TO IMPACT AGAINST SHARP OBJECTS

MARA PAGANI* **and UMBERTO PEREGO***

*Department of Structural Engineering
Politecnico di Milano
Piazza Leonardo da Vinci, 20133 Milan, Italy
e-mail: pagani@stru.polimi.it, umberto.perego@polimi.it

Key words: Cohesive Elements, Crack Propagation, Solid-Shell Elements

Abstract. The present paper is concerned with the development of an effective finite element tool for the simulation of crack propagation in thin structures, induced by contact or impact against sharp objects. In particular the purpose is the refinement and further development of a recently proposed finite element approach for the simulation of the blade cutting of thin membranes [1]. Standard cohesive interface elements are not suited for the simulation of this type of cutting, dominated by the blade sharpness and by large failure opening of the cohesive interface. The new concept of "directional" cohesive element, to be placed at the interface between adjacent shell elements, where the cohesive forces can have different directions on the two sides of the crack whenever the cohesive region is crossed by the cutting blade, was introduced in [1] for elastic 4-node full-integration shell elements with dissipation localized inside the interface elements, in the framework of an explicit dynamics formulation. In the present paper the computational efficiency of the proposed approach is investigated by considering applications to different test problems, modifying the shell element kinematics. Some considerations about a reduced integration solid-shell element are here reported; the interaction between this kind of element and directional cohesive elements is under study.

1 INTRODUCTION

Thin structures are typically modeled using shell finite elements. Since many years, most explicit commercial finite element codes (see e.g. Abaqus and LS-Dyna) offer the possibility to simulate crack propagation in shells by eliminating from the model those finite elements where developing damage has reached a critical threshold. While this approach provides good results for the simulation of diffused damage due to explosions or crashes against large obstacles, it is not convenient for the simulation of the propagation of isolated cracks in large structures or of localized damages produced by sharp obstacles

(see e.g. [2]). This type of problems appear to be better tackled by approaches based on the use of cohesive fracture models, capable to transmit cohesive forces across either an intra-element or inter-element displacement discontinuity [3],[4]. Among the different types of crack propagation problems in thin structures, the mechanics of cutting a shell with a sharp object or tool has attracted particular attention in view of its engineering interest [5]. Standard cohesive interface elements are not suited for the simulation of this type of cutting, dominated by the blade sharpness and by large failure opening of the cohesive interface. The new concept of "directional" cohesive element, to be placed at the interface between adjacent shell elements, where the cohesive forces can have different directions on the two sides of the crack whenever the cohesive region is crossed by the cutting blade, was introduced in [1] for elastic shells with dissipation localized inside the interface elements, in the framework of an explicit dynamics formulation. In the present paper the proposed approach is briefly summarized and used to simulate the cutting of a thin rubber sheet, on the basis of the experimental test discussed in [6]. In [1] the interface element was applied in conjunction with full integration 4-node shell elements (MITC4 elements [7]). For future application to elastoplastic laminated shells, the kinematics of a computationally effective reduced integration solid shell element is discussed and its possible use in the present explicit dynamics context is investigated.

2 COHESIVE ELEMENTS

2.1 Model description

In standard finite element approaches to fracture, based on the introduction of a cohesive interface between adjacent shell elements, due to the crack propagation opposite cohesive forces develop across the displacement discontinuity. The direction of the opposite forces depends only on the direction of the displacement jump and on the adopted cohesive law. When the material is quasi-brittle and/or the impacting object is blunt, there is no interference between the object and the cohesive region because the ultimate cohesive opening displacement is much smaller than the typical size of the cutter. On the contrary, when the material is very ductile or the cutting blade is sharp, it may well happen that the blade intersects the trajectory of the cohesive forces, giving rise to inaccurate predictions of the crack propagation. For these reasons, a new concept of "directional" cohesive interface element, where the cohesive forces acting on the crack opposite faces have different directions when the process zone is crossed by the cutting blade, has been proposed in [1] and is briefly recalled below.

The implementation of these "directional" cohesive elements follows the following steps. When the selected fracture criterion is met at a given node, the node is duplicated and it is assumed that cohesive forces $\mathbf{F}_i^{\pm}$ are transmitted between the newly created pair of nodes $i^{\pm}$ by a massless "cable", i.e. a truss element ad hoc introduced in the model in correspondence of each pair of separating nodes. In the current implementation, the cohesive cables are attached to nodes lying in the middle surface of the shell. Contact of

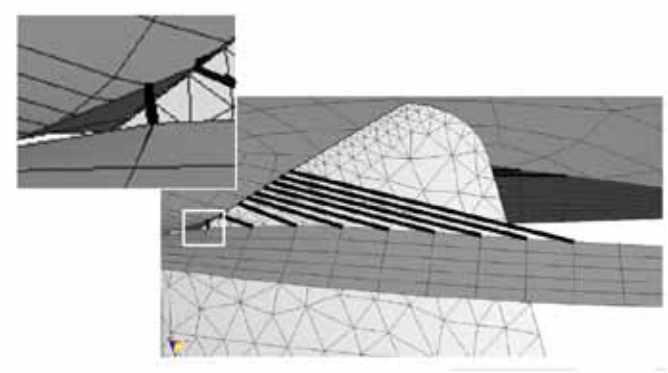

Figure 1: Cohesive forces between detaching elements.

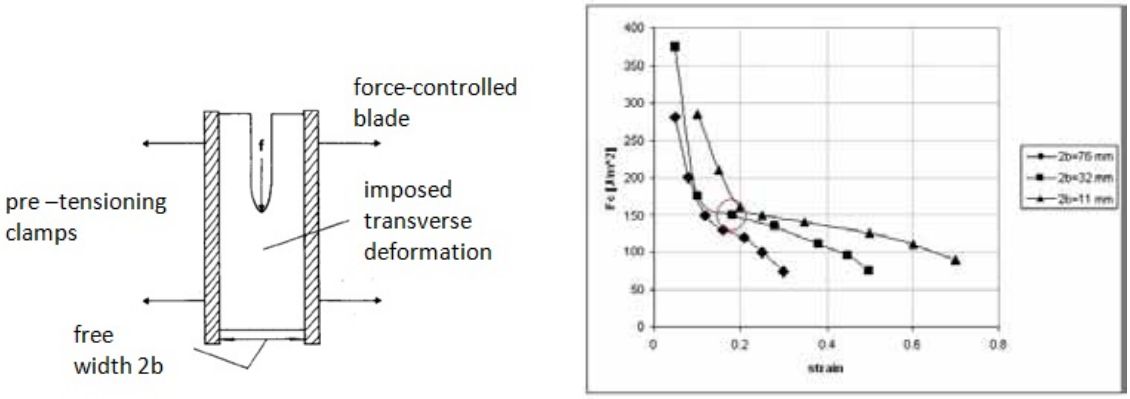

(a) (b)

Figure 2: Cutting of a rubber sheet: (a) test setup and (b) experimental results.

cable elements (which are geometric entities) against the cutting blade is checked. When a point of a cable element is detected to be in contact with the blade, the cable element is subdivided into two elements by introducing a joint in correspondence of the contact point (see Fig. 1). The force transmitted by the cables depends on their length (rather than on the distance between opposite crack nodes as in standard cohesive elements) according to the adopted cohesive law. When the current total cable length exceeds the limit value, the cable is removed and no forces are anymore transmitted between the opposite nodes.

2.2 Model validation

In order to validate this new approach, the force-controlled cutting of a pre-tensioned rubber sheet is simulated. The test setup and the recorded [6] cutting force at unstable propagation onset are shown in Fig. 2 for varying pre-tensioning and rubber sheet width. The test geometry and mesh shown in Fig. 3a have been considered, with length $L =$

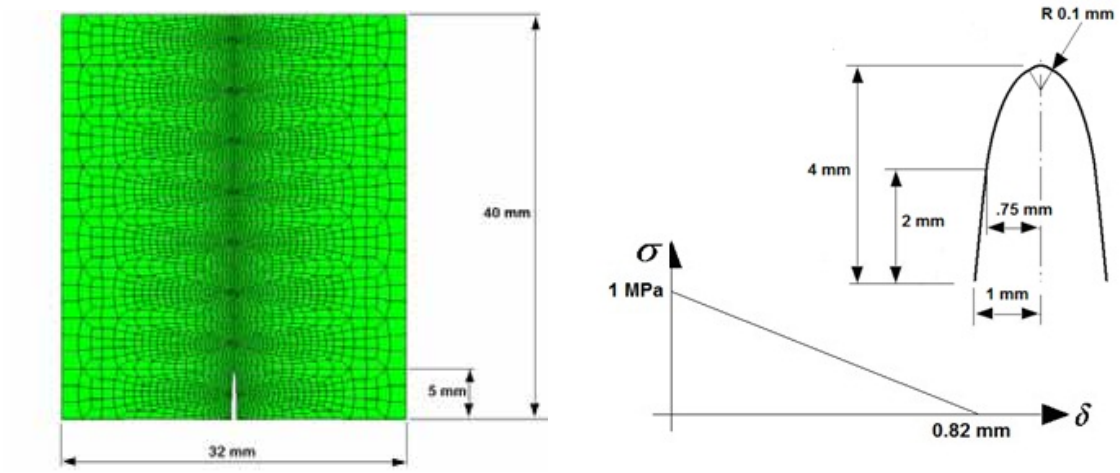

(a) (b)

Figure 3: Cutting of a rubber sheet: (a) dimensions and mesh of the rubber sheet and (b) cohesive law and blade shape.

40 mm, width $D = 32$ mm, thickness $t = 0.1$ mm, initial defect $a = 5$ mm, Young modulus $E = 1$ MPa, Poisson ratio $\nu = 0.45$ and the cohesive law shown in Fig. 3b. Imposing a transverse tensile strain of 18%, a cutting force at unstable crack propagation equal to about 150 N/m is expected to be obtained (see circled dot in Fig. 2b).

The numerical results of the explicit dynamics simulation are shown in Fig. 4. The first plot shows the evolution of the vertical reaction force at the lateral clamps. The first part of the plot concerns the initial pre-tensioning phase. The second part concerns the cutting phase. The second plot shows the time evolution of the contact force at the blade tip. As it can be observed, this oscillates about the experimentally measured value of 0.015 N, which confirms the good accuracy of the simulation.

3 SOLID-SHELL ELEMENTS

The MITC4 shell elements used in the previous example need four integration points in the shell plane and at least two integration points along the thickness for a total of eight integration points. The introduction of material non-linearities, requires a higher number of Gauss points, leading to increasing computational costs.

Several types of 8-node solid-shell elements have been recently proposed in the literature. Among these, the SHB8PS element proposed by Abed-Meraim and Combescure [9] has eight nodes, only one integration point in the plane and an arbitrary number of integration points, with a minimum of two, distributed along the thickness direction and it is based on the assumed strain stabilization proposed by Belytschko and Bindeman[8]. Combescure's element is here reconsidered with some modifications aimed at improving its computational effectiveness, especially in explicit dynamics analyses (see [9] for a detailed

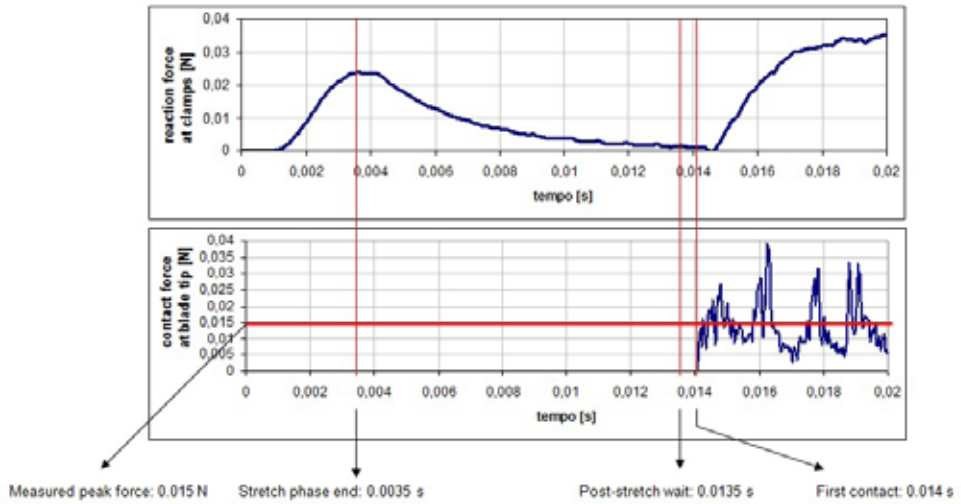

Figure 4: Cutting of a rubber sheet. Numerical results: vertical reaction force evolution at lateral clamps (upper plot); evolution of contact force at cutter tip (lower plot).

SHB8PS element presentation).

3.1 SHB8PS element

SHB8PS is a hexahedral, 8-node, isoparametric element with three-linear interpolation. It makes use of a set of n_{int} integration points distributed along the ζ direction in the local coordinate frame as shown in Fig. 5.

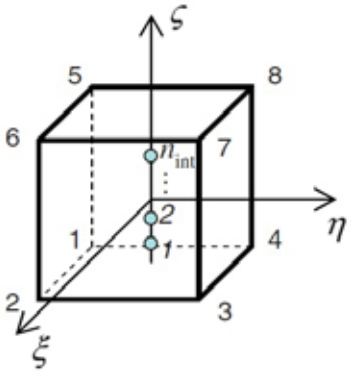

node	ξ	η	ζ
1	-1	-1	-1
2	1	-1	-1
3	1	1	-1
4	-1	1	-1
5	-1	-1	1
6	1	-1	1
7	1	1	1
8	-1	1	1

Figure 5: SHB8PS reference geometry, integration points location and nodal coordinates.

Indicating with $\mathbf{d}_i$ and $\mathbf{x}_i$ the vectors of nodal displacements and coordinates for each element, Belytschko and Bindeman have shown that the nodal displacements can be

expressed as :

$$\mathbf{d}_i = a_{01}\mathbf{s} + a_{1i}\mathbf{x}_1 + a_{2i}\mathbf{x}_2 + a_{3i}\mathbf{x}_3 + c_{1i}\mathbf{h}_1 + c_{2i}\mathbf{h}_2 + c_{3i}\mathbf{h}_3 + c_{4i}\mathbf{h}_4 \tag{1}$$

where

$$\begin{array}{l}
\mathbf{s}^T = (1,1,1,1,1,1,1,1) \\
\mathbf{h}_1^T = (1,1,-1,-1,-1,-1,1,1) \\
\mathbf{h}_2^T = (1,-1,-1,1,-1,1,1,-1) \\
\mathbf{h}_3^T = (1,-1,1,-1,1,-1,1,-1) \\
\mathbf{h}_4^T = (-1,1,-1,1,1,-1,1,-1) \\
a_{ji} = \mathbf{b}_j^T \cdot \mathbf{d}_i, \qquad c_{\alpha i} = \boldsymbol{\gamma}_\alpha^T \cdot \mathbf{d}_i, \qquad i,j = 1\ldots 3
\end{array}$$

and $\boldsymbol{\gamma}_\alpha$ and the mean form $\mathbf{b}_i$ of Flanagan and Belytschko [10] are defined as ($\mathbf{N}$ being the shape functions):

$$\begin{array}{l}
\boldsymbol{\gamma}_\alpha = \dfrac{1}{8}\left[\mathbf{h}_\alpha - \displaystyle\sum_{j=1}^{3}(\mathbf{h}_\alpha^T \cdot \mathbf{x}_j)\mathbf{b}_j\right], \qquad \alpha = 1,\ldots,4 \\
\mathbf{b}_i = \frac{1}{\Omega_e}\int_{\Omega_e} \mathbf{N}_{,i}(\xi,\eta,\zeta)\mathrm{d}\Omega, \qquad i = 1,2,3
\end{array} \tag{2}$$

Defining the four functions

$$h_1 = \eta\zeta, \quad h_2 = \zeta\xi, \quad h_3 = \xi\eta, \quad h_4 = \xi\eta\zeta \tag{3}$$

this allows to express the discrete gradient operator relating the strain field to the nodal displacements as

$$\begin{array}{rcl}
\nabla(\mathbf{u}) & = & \mathbf{B}\cdot\mathbf{d} \qquad \text{with} \\
\mathbf{B} & = & \left[\begin{array}{ccc}
\mathbf{b}_x^T + h_{\alpha,x}\boldsymbol{\gamma}_\alpha^T & \mathbf{0} & \mathbf{0} \\
\mathbf{0} & \mathbf{b}_y^T + h_{\alpha,y}\boldsymbol{\gamma}_\alpha^T & \mathbf{0} \\
\mathbf{0} & \mathbf{0} & \mathbf{b}_z^T + h_{\alpha,z}\boldsymbol{\gamma}_\alpha^T \\
\mathbf{b}_y^T + h_{\alpha,y}\boldsymbol{\gamma}_\alpha^T & \mathbf{b}_x^T + h_{\alpha,x}\boldsymbol{\gamma}_\alpha^T & \mathbf{0} \\
\mathbf{0} & \mathbf{b}_z^T + h_{\alpha,z}\boldsymbol{\gamma}_\alpha^T & \mathbf{b}_y^T + h_{\alpha,y}\boldsymbol{\gamma}_\alpha^T \\
\mathbf{b}_z^T + h_{\alpha,z}\boldsymbol{\gamma}_\alpha^T & \mathbf{0} & \mathbf{b}_x^T + h_{\alpha,x}\boldsymbol{\gamma}_\alpha^T
\end{array}\right]
\end{array} \tag{4}$$

For a set of n_{int} integration points ($I = 1,\ldots,n_{int}$), with coordinates $\xi_I = \eta_I = 0, \zeta \neq 0$, the derivatives $h_{\alpha,i}$ ($\alpha = 3,4; i = 1,2,3$) vanish, so that (4) reduces to a matrix $\mathbf{B}_{12}$ where the sum on the repeated index α only goes from 1 to 2, leading to six hourglass modes in the element stiffness matrix $\mathbf{K}_e$:

$$\mathbf{K}_e = \int_{\Omega_e} \mathbf{B}^T \cdot \mathbf{C} \cdot \mathbf{B}\mathrm{d}\Omega = \sum_{I=1}^{n_{int}} \omega(\zeta_I) J(\zeta_I) \mathbf{B}^T(\zeta_I) \cdot \mathbf{C} \cdot \mathbf{B}(\zeta_I) \tag{5}$$

where $\omega(\zeta_I)$ are Gauss' weights, $J(\zeta_I)$ is the geometry Jacobian, and $\mathbf{C}$ the matrix of elastic moduli.

The stabilization of the hourglass modes is obtained assuming a modified compatibility operator $\bar{\mathbf{B}}$:

$$\bar{\mathbf{B}} = \mathbf{B}_{12} + \mathbf{B}_{34} \tag{6}$$

where $\mathbf{B}_{34}$ is a stabilization term, computed in a co-rotational system, having the following expression [9]:

$$\mathbf{B}_{34} = \begin{bmatrix} \sum_{\alpha=3}^{4} h_{\alpha,x}\boldsymbol{\gamma}_\alpha^T & \mathbf{0} & \mathbf{0} \\ \mathbf{0} & \sum_{\alpha=3}^{4} h_{\alpha,y}\boldsymbol{\gamma}_\alpha^T & \mathbf{0} \\ \mathbf{0} & \mathbf{0} & h_{3,z}\boldsymbol{\gamma}_3^T \\ \mathbf{0} & \mathbf{0} & \mathbf{0} \\ \mathbf{0} & \mathbf{0} & \mathbf{0} \\ \mathbf{0} & \mathbf{0} & h_{4,x}\boldsymbol{\gamma}_4^T \end{bmatrix} \tag{7}$$

The elastic stiffness matrix is then given by the sum of the following contributions:

$$\mathbf{K}_{12} = \int_{\Omega_e} \mathbf{B}_{12}^T \cdot \mathbf{C} \cdot \mathbf{B}_{12} \mathrm{d}\Omega = \sum_{I=1}^{n_{int}} \omega(\zeta_I) J(\zeta_I) \mathbf{B}_{12}^T(\zeta_I) \cdot \mathbf{C} \cdot \mathbf{B}_{12}(\zeta_I) \tag{8}$$

$$\mathbf{K}_{STAB} = \int_{\Omega_e} \mathbf{B}_{12}^T \cdot \mathbf{C} \cdot \mathbf{B}_{34} \mathrm{d}\Omega + \int_{\Omega_e} \mathbf{B}_{34}^T \cdot \mathbf{C} \cdot \mathbf{B}_{12} \mathrm{d}\Omega + \int_{\Omega_e} \mathbf{B}_{34}^T \cdot \mathbf{C} \cdot \mathbf{B}_{34} \mathrm{d}\Omega \tag{9}$$

The stabilization terms are evaluated in a co-rotational system allowing to compute the integrals analytically, in this way improving accuracy and saving computing time.

3.2 Enhanced Assumed Strain EAS

Solid-shell elements are well known to be affected by volumetric locking and by the so-called Poisson thickness locking. Volumetric locking occurs when the material approaches incompressibility. Poisson thickness locking reveals itself in out-of-plane bending, e.g. about the η-axis (see Fig. 6). The analytical solution of the problem leads to a transverse normal strain $\varepsilon_{\zeta\zeta}$, which is constant within the shell plane but linear in the thickness direction ζ, while the assumed displacement model leads to $\varepsilon_{\zeta\zeta}$ constant through the thickness. To avoid Poisson thickness locking and volumetric locking, the strain terms $\varepsilon_{\xi\xi}$, $\varepsilon_{\eta\eta}$ and $\varepsilon_{\zeta\zeta}$ must be modeled through the thickness by polynomials of the same order. This can be achieved by enhancing the strain component $\varepsilon_{\zeta\zeta}$ in ζ direction by use of the EAS concept, as proposed e.g. in [11] and [12]. The covariant strain enhancement is expressed as

$$\boldsymbol{\varepsilon}_{enh} = \mathbf{B}_{enh} W_{enh} \tag{10}$$

where

$$\mathbf{B}_{enh} = [0, 0, \zeta, 0, 0, 0]^T \tag{11}$$

and W_{enh} is the enhancement degree-of-freedom of the considered element, which enriches $\varepsilon_{\zeta\zeta}$ linearly in ζ. The computationally inexpensive EAS approach avoids to make use of the modified plane-stress elastic tensor, used to this purpose in [9], which requires the definition of an additional material co-rotational reference frame.

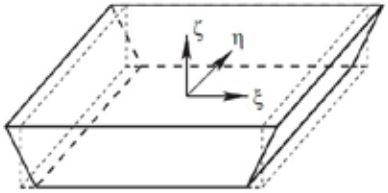

Figure 6: Bending about η-axis.

Application of the enhanced SHB8PS element to the cantilever plate strip under a tip load proposed in [13] (see Fig. 7) produces the results shown in Fig. 8.

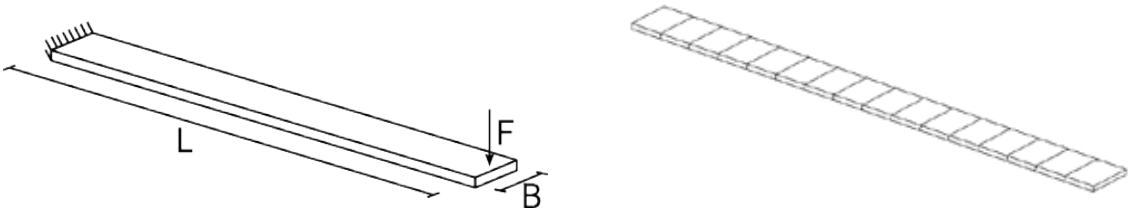

(a) (b)

Figure 7: Cantilever plate strip: (a) geometry and load; (b) mesh.

Table 1: Plate strip parameters

L	B	T	E
10 mm	1 mm	0.1 mm	10^7 N/mm^2

The plate strip is characterized by the geometric and material parameters reported in Table 1. The small-displacements out-of-plane bending behavior in the near incompressible limit is studied. The mesh consists of 16 regular elements while a total tip force of 40 N is applied in 10 time steps. Poisson's ratio is varied between $\nu = 0$ and $\nu = 0.499$, and load vs. displacement diagrams are shown in Figs. 8. It can be noted that while the SHB8PS element without any correction of the behavior in the thickness direction is

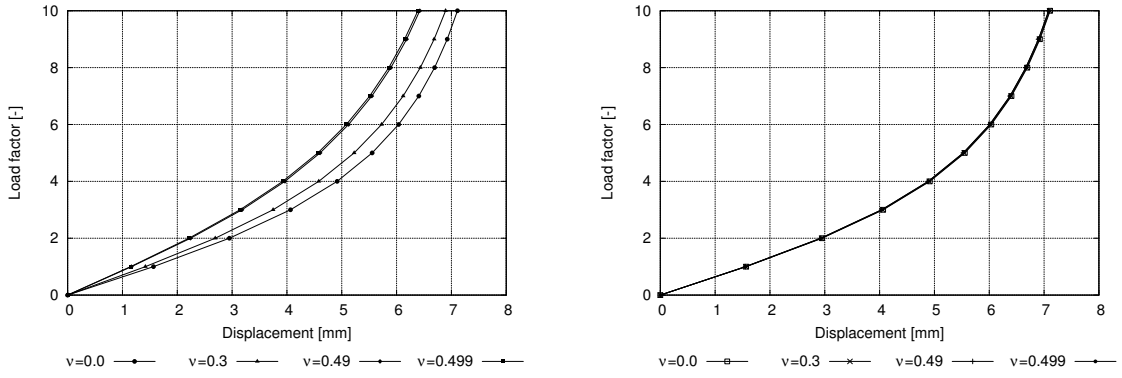

Figure 8: Cantilever plate strip under tip load: (a) SHB8PS element without EAS enhancement; (b) with EAS enhancement.

sensitive to Poisson's ratio variations (Fig. 8a), complete insensitivity of the response is shown by its enhanced version (Fig. 8b). A similar insensitivity is also obtained using the modified plane-stress elastic tensor as proposed in [9], though at the cost of computing a new co-rotational frame at each increment.

3.3 Element modification for explicit dynamics

For application to problems of the type considered in section 2, with contact and crack propagation, explicit dynamics approaches are usually preferred. However, the incorporation of solid-shell elements into an explicit code leads to very small time increments due to the element small thickness compared to the in-plane dimensions. Time-step sizes of the same order of magnitude of those required by normal shell elements, such as the MITC4 used in section 2, can be obtained by means of a variable transformation, where new translational and rotational degrees of freedom in the element middle plane are introduced according to the following definition:

$$\mathbf{u}_i = \frac{\mathbf{u}_a + \mathbf{u}_b}{2} \qquad i = 1,\dots,4 \qquad a = 1,2,3,4 \qquad b = 5,6,7,8 \tag{12}$$

$$\boldsymbol{\phi}_i = \frac{\mathbf{u}_b - \mathbf{u}_a}{2} \qquad i = 1,\dots,4 \qquad a = 1,2,3,4 \qquad b = 5,6,7,8 \tag{13}$$

$$\tag{14}$$

where $a = 1,2,3,4$ and $b = 5,6,7,8$ indicate nodes belonging to the lower and upper element faces, respectively, as depicted in Fig. 5. In this way it is possible to introduce a selective scaling of masses corresponding to the ϕ_i degrees of freedom, as is usually done in shell elements [14]. The effectiveness of this provision is studied by simulating the cantilever beam described in Fig. 9, impulsively loaded by a uniformly distributed transverse load. The beam has length $L = 10$ mm, a rectangular cross section of width

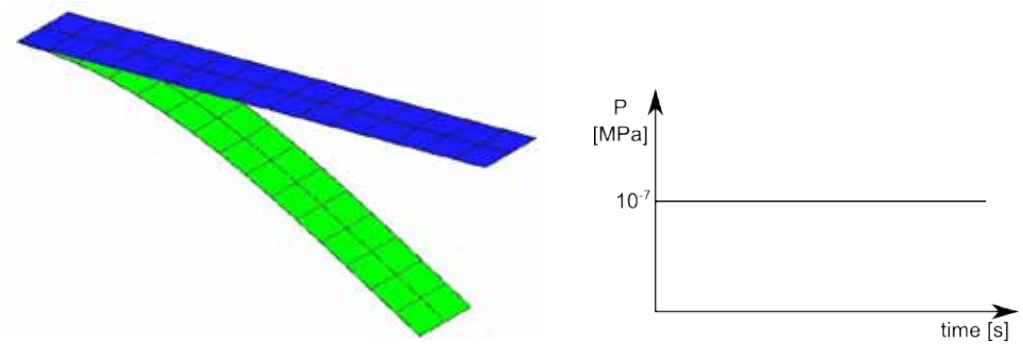

(a) (b)

Figure 9: Impulsively loaded cantilever beam: (a) Finite element undeformed/deformed mesh and (b) applied load.

$B = 2.5$ mm and thickness $T = 0.0074$ mm, Young modulus $E = 1768$ MPa, Poisson ratio $\nu = 0.3$, density $\rho = 3 \cdot 10^{-9}$ T/mm^3. The problem has been analyzed using three different types of elements: MITC4, SHB8PS and improved SHB8PS. The stable time increments obtained in the three cases according to Gerschgorin's theorem are reported in Table 2. It can be seen that the SHB8PS with transformed degrees of freedom leads to a stable time step of the same order of the MITC4, two orders of magnitude smaller than the standard SHB8PS. The displacement evolution of the beam tip, obtained by MITC4 and improved SHB8PS elements, is shown in Fig. 10. An almost complete agreement between the two analyses can be observed.

Table 2: Stable time increments

Element type	**Time increment**
MITC4	$5.17 \cdot 10^{-7}$ s
SHB8PS	$7.26 \cdot 10^{-9}$ s
Improved SHB8PS	$5.95 \cdot 10^{-7}$ s

4 CONCLUSIONS

The development of an effective numerical tool for the simulation of the cutting process of thin membranes has been discussed. It has been shown how the cutting of a rubber pre-tensioned membrane can be accurately simulated by using "directional" cohesive elements in conjunction with standard shell elements. In a more general case, inelastic dissipation due to plasticity and delamination takes place in the cutting region of thin laminates. The description of these nonlinear phenomena is more conveniently achieved by using solid-shell elements. Reference has been made to the SHB8PS element [9], recently proposed

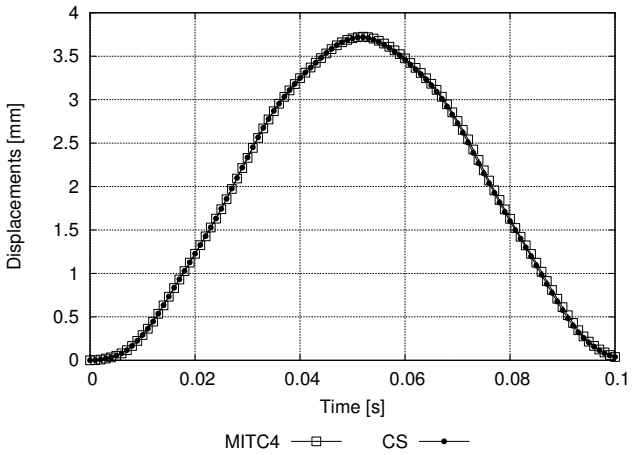

Figure 10: Impulsively loaded cantilever beam: tip displacements evolution obtained by MITC4 and SHB8PS elements.

in the literature. Two modifications of the element have been proposed to improve its performance: the adoption of an enhanced strain approach in the thickness direction, to avoid volume locking and Poisson's thickness locking, and a linear variable transformation, to allow for mass scaling and consequent increase of the time-step size in explicit dynamics. The application of this modified solid-shell element to cutting problems is currently in progress.

REFERENCES

[1] Frangi, T., Pagani, M., Perego, U. and Borsari, R. Directional Cohesive Elements for the Simulation of Blade Cutting of Thin Shells. *Computer Modeling in Engineering & Sciences*. (2010) **57:3**:205-224.

[2] Iqbal, M.A., Gupta, G. and Gupta, N.K. 3D numerical simulations of ductile targets subjected to oblique impact by sharp nosed projectiles. *International Journal of Solids and Structures*. (2010) **47(2)**:224-237.

[3] Song, J.H. and Belytschko, T. Dynamic fracture of shells subjected to impulsive loads. *Journal of Applied Mechanics*. (2009) **76**:051301_1 051301_9.

[4] Areias, P.M.A., Song, J.H. and Belytschko, T. Analysis of fracture in thin shells by overlapping paired elements. *Computer Methods in Applied Mechanics and Engineering*. (2006) **95(41-43)**:53435360.

[5] Atkins, T. *The science of engineering of cutting*. Buttenworth Heinemann, (2009).

[6] Lake, G. J. and Yeoh, O. H. Measurement of rubber cutting resistance in the absence of friction. *International Journal of Fracture* (1978) **14(5)**:509-526.

[7] Bathe, K. *Finite element procedures*. Prentice-Hall Int., Englewood Cliffs, NJ, USA, (2009).

[8] Belytschko, T. and Bindeman, L.P. Assumed strain stabilization of the eight node hexahedral element. *Computer Methods in Applied Mechanics and Engineering*. (1993) **105**:225-260

[9] Abed-Meraim, F. and Combescure, A. An improved assumed strain solid-shell element formulation with physical stabilization for geometric non-linear applications and elastic-plastic stability analysis. *International Journal for Numerical Methods in Engineering*. (2009) **80**:1640-1686.

[10] Flanagan, D. P. and Belytschko, T. A uniform strain hexahedron and quadrilateral with orthogonal hourglass control, *International Journal for Numerical Methods in Engineering*. (1981) **17(5)**:679-706.

[11] Schwarze, M. and Reese, S. A reduced integration solid-shell finite element based on the EAS and the ANS concept-Geometrically linear problems. *International Journal for Numerical Methods in Engineering*. (2009) **80**:1322-1355.

[12] Cardoso, R.P.R., Yoon, J.W., Mahardika, M., Choudhry, S., Alves de Sousa, R.J. and Fontes Valente, R.A. Enhanced assumed strain (EAS) and assumed natural strain (ANS) methods for one-point quadrature solid-shell elements. *International Journal for Numerical Methods in Engineering*. (2008) **75**:156-187.

[13] Schwarze, M. and Reese, S. A reduced integration solid-shell finite element based on the EAS and the ANS concept-Large deformation problems. *International Journal for Numerical Methods in Engineering*. (2010) **85**:289-329.

[14] Key, S.W. and Beisinger, Z.E. Transient Dynamic Analysis of Thin Shells by Finite Element Methods. *Proceedings of Third Conference Matrix Methods in Structural Analysis*, Wright-Patterson Air Force Base, Ohio (1971) .